Magnetic energies of single submicron permalloy rectangles determined via magnetotransport

André Kobs,* Hendrik Spahr, Daniel Stickler, Sebastian Hankemeier, Robert Frömter, and Hans Peter Oepen
Institut für Angewandte Physik, Universität Hamburg, Jungiusstraße 11, 20355 Hamburg, Germany
(Received 31 March 2009; revised manuscript received 22 September 2009; published 19 October 2009)

We have investigated the magnetic properties of single submicron permalloy rectangles with a thickness of 20 nm and an aspect ratio of 2:1 via anisotropic magnetoresistance (AMR). Preparation and investigation via magnetotransport are performed *in situ* in ultrahigh vacuum. The field-dependent magnetization behavior of the two generic cases with the magnetic field applied perpendicular and parallel to the long axis of the rectangles is studied. Due to the high sensitivity of our setup, single field sweeps are sufficient to obtain magnetoresistance curves of structures with dimensions as small as 600×300 nm^2. To link features of the AMR to changes in the micromagnetic states, the remanent state has been investigated via scanning electron microscopy with polarization analysis. Our main result is that the energy density of micromagnetic states can be obtained from the hard-axis magnetization behavior. It is demonstrated that a C/S state can be distinguished from a Landau state and the energy difference between both states is determined.

DOI: 10.1103/PhysRevB.80.134415 PACS number(s): 75.60.−d, 75.50.Bb, 75.47.−m, 81.16.−c

I. INTRODUCTION

Present basic research on magnetism is mainly focused on nanostructures, particularly their fabrication and characterization. The ultimate aim is to understand the magnetization behavior of nanostructures and to follow the transition from collective behavior to the quantum-mechanical behavior of atoms and molecules. In a bottom up approach, i.e., depositing single atoms, clusters, or nanoislands on perfect surfaces, big progress has been made over the last years, which is enabled by the improvements of scanning probe techniques.[1–3] A disadvantage of this approach is caused by the method of preparation of the nanosized elements, as it does not allow to tune magnetic or structure parameters on purpose. Therefore, a systematic evaluation of dependences is not possible. A further problem is the fact that magnetic properties are only indirectly accessible via modeling the lateral distribution of the probed quantities. In general, imaging techniques with high spatial resolution are utilized to study the domain pattern.[4] Modeling the domain structure then allows to extract indirectly the magnetic quantities.

The top-down approach, i.e., the fabrication of artificial nanostructures, has also made tremendous progress in recent times.[5] However, the characterization of such structures is still lagging behind because the quantitative analysis of single structures is difficult due to missing sensitivity of conventional characterization techniques. To study, e.g., the size and shape dependence of magnetic properties of single nanostructures, new methods have to be developed. The route to achieve the required sensitivity for measuring magnetic properties of single nanostructures is via miniaturized probes that are combined with conventional macroscopic measurement tools. The pioneering experiment in this field was the successful measurement of magnetic-flux density via microsuperconducting quantum interference device.[6] Nowadays the trend is shifting toward investigating magnetic wires, which are of technological relevance.[7,8] Measuring the anisotropic magnetoresistance (AMR) of wires with two dimensions shrank to the nanoscale has the potential to sensitively detect the switching fields.[9–12] Until recently, the reversal has been interpreted in the framework of homogenous magnetization reversal of the whole wire, as predicted analytically for rotational ellipsoids.[13] On the contrary, latest investigations have demonstrated that the assumption of nonlocal reversal procedures is wrong.[14,15] Instead, a domain wall nucleates at the end of the wire and rushes through the wire, as predicted theoretically.[16,17] This example demonstrates that the combination of domain structure investigation and quantitative studies of switching fields, anisotropies, or other magnetic quantities is mandatory.

While single wires are frequently investigated, the study of real nanostructures (all three dimensions nanosized) is rare and most often performed with the help of nanostructure arrays.[18,19] To address an individual nanostructure is very demanding as the whole measuring device has to be scaled down. In this paper we present an approach for AMR investigation of single structures with lateral dimensions down to some 100 nm. Additionally, this approach gives the flexibility to vary parameters of the nanostructure, such as size and shape, which opens the way to systematically study dependences on particular parameters.

In this paper we demonstrate how this technique allows to quantify the size-dependent energy of the Landau state in single nanostructures below 1 μm lateral size. The quantitative magnetization behavior obtained via AMR is complemented by domain structure investigations via scanning electron microscopy with polarization analysis (SEMPA). The combination of both methods gives direct access to the understanding of the reversal mode and the resultant interpretation.

II. EXPERIMENTAL DETAILS

The experiments are performed in a UHV dual beam system, equipped with a focused ion beam (FIB) and a SEM. The FIB is used to create a microsized electrical circuit including a ferromagnetic rectangle in a film [see Fig. 1(a)]. For the *in situ* magnetoresistance measurements the electrical circuit is contacted by a micromanipulator.[20] The current is driven through the structure to the film, which serves as sec-

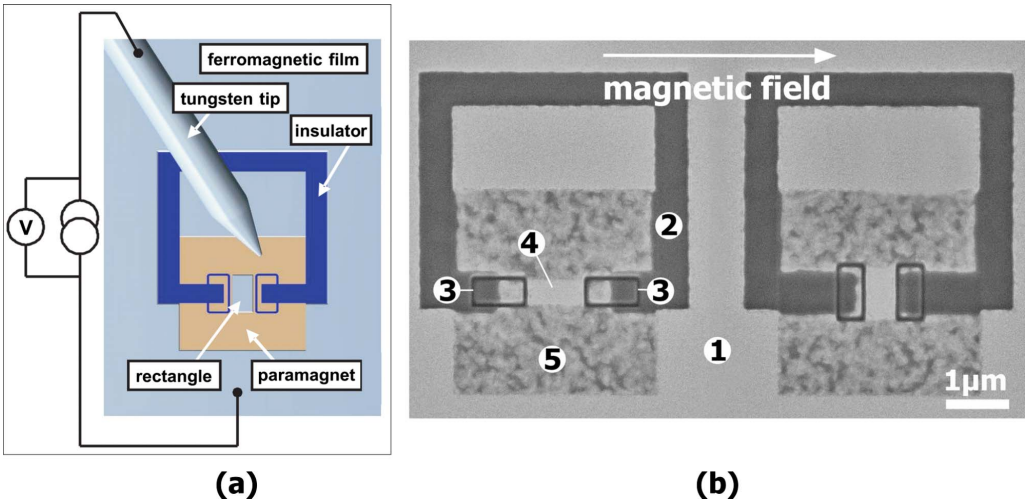

FIG. 1. (Color online) Microsized circuits for magnetoresistance measurements. (a) Sketch of the measurement principle. The tungsten tip can be moved by a micromanipulator to contact the circuit within the framed region. The approach is monitored via SEM. The current is driven from the tip to the film crossing a small ferromagnetic rectangle within the gap of the yoke-shaped frame. (b) SEM micrograph of two microsized circuits with different orientations of the ferromagnetic rectangles (4) with respect to the field direction (arrow). The rectangles of size 800×400 nm^2 are surrounded by paramagnetic material (5), which has been created by Ga^+ ion bombardment out of the ferromagnetic film (1). The dark gray parts (2, 3), where the metal has been totally removed by sputtering, are electrically insulating.

ond electrode. A magnetic field of up to ±23 mT can be applied within the film plane. The orientation of the magnetic field is fixed with respect to the sample. The fabrication process and tip steering is controlled via SEM. The dimensions of the investigated rectangles are 1000×500, 800×400, and 600×300 nm^2. The energy of the Ga^+ ions is 30 keV at a beam current of 40 pA.

An SEM image of two FIB made microcircuits is shown in Fig. 1(b). The bright gray regions show the unperturbed film (1). In the black areas (2, 3) the metal has been completely removed by ion milling. The FIB preparation is performed in three steps: in the first step a yoke-shaped structure (2) is milled, which isolates the framed region from the film (1) except for the small part in the gap of the yoke. In the second step the rectangle (4) in the gap of the yoke is created. For that purpose, the area around the rectangle is irradiated by Ga^+ ions (5) to destroy the long-range magnetic order while conductance is maintained. Narrow isolation lines (3) are prepared in the third step close to the rectangle (nominal distance of 75 nm) so that almost the whole current has to pass through the rectangle and any bypassing current is kept negligibly small. This layout creates the highest current density of the whole electrical circuit in the region of the rectangle, which enhances the sensitivity for the ferromagnetic structure. This preparation procedure guarantees the most precise geometry of the rectangle as any distortion due to thermal drift is minimized. The second microsized circuit on the right-hand side in Fig. 1(b) has a different orientation of the rectangle with respect to the magnetic field and current direction.

For the experiments a Cr (10 nm)/Py (20 nm)/Pt (2.5 nm) multilayer film is used, which has been deposited on an electrically insulating Si_3N_4 substrate using electron-beam evaporation. The deposition rate is 0.5 Å/s at a base pressure of 10^{-8} mbar. The Cr layer serves as a seed layer while the Pt layer on top prevents oxidation.

When destroying the long-range magnetic order by ion bombardment, it is necessary to maintain a low resistance of the leads (5) to keep the sensitivity for magnetogalvanic effects high. This can be achieved by keeping the material removal as small as possible. For that purpose the Cr layer is incorporated into the multilayer stack to induce intermixing of permalloy (Py) and Cr by ion bombardment.[21] As only 8% of Cr in Py causes the Py to become paramagnetic at room temperature,[22,23] the phase transition should be achieved already at low ion doses. For the layer system a gallium ion dose of 6000 μC/cm^2 (3.75×10^{16} Ga^+/cm^2) is needed to destroy long-range order while a film thickness of only about 12 nm is removed (to be published).

The magnetoresistance is measured utilizing pulsed electrical currents with an amplitude of $I=0.3$ mA (duty cycle of 10%), which corresponds to maximum current densities of 3×10^{10} A/m^2. This current density does not cause any detectable heating of the submicron structure[20] and is about one order of magnitude smaller than required to move domain walls in Py.[24] As mentioned above, two different orientations of the rectangles with respect to the magnetic field direction are fabricated while the orientation of the microsized circuit is not changed. This enables the investigation of the two generic cases with the magnetic field applied parallel to the long and short axis of the rectangle, respectively, while current and field are orientated perpendicular to each other.

After the MR measurements the magnetic microstructure has been investigated by means of SEMPA.[25] As the rectangles have two different orientations with respect to the magnetic field, the micromagnetic structure in remanence is obtained for both pretreatments.

III. RESULTS AND DISCUSSION

In a first step, we have checked for parasitic contributions to the resistance due to magnetogalvanic effects in the whole

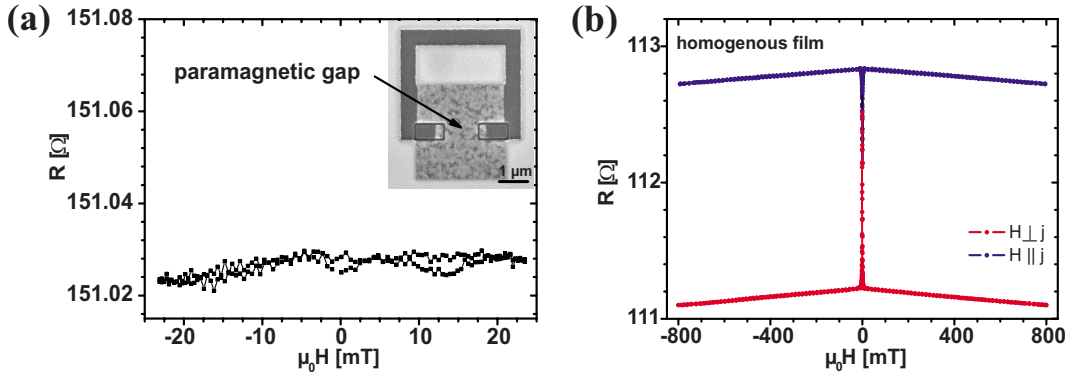

FIG. 2. (Color online) Resistance versus field curves. (a) MR measurement of a paramagnetic gap. An SEM micrograph of the microsized circuit is shown as inset. (b) MR measurements of the film system. The measurements are performed on a macroscopic wire with dimensions of $l=6$ mm and $w=0.5$ mm. The current is driven through the whole wire while the voltage drop along 4 mm is measured. The magnetic field is applied in the film plane perpendicular ($H \perp j$) and parallel ($H \| j$) to the current direction, respectively. At low fields the AMR dominates due to magnetization reversal processes. At high fields the isotropic negative MR dominates, which is due to the decrease in spin-wave density on field increase.

circuit including the ferromagnetic film. For that purpose we have created a circuit with identical layout while the rectangle has been rendered paramagnetic in the same way as explained above [see inset of Fig. 2(a)]. The obtained resistance versus magnetic field curve is plotted in Fig. 2(a). Within the resolution of the measurement ($\Delta R/R=1\times10^{-5}$) no dependence of the resistance on the magnetic field is found. This result demonstrates that any MR signal arising from the ferromagnetic film can be neglected. Additionally, it proves that the applied ion dose is sufficient to destroy ferromagnetism. In comparison to the MR curves obtained for the rectangles (see below) this result also shows the high sensitivity for the ferromagnetic nanostructures.

In a second step, we have characterized the MR properties of the homogeneous film in an *ex situ* four-point MR setup in magnetic fields of up to ±800 mT. The dependence of the resistance on field is plotted in Fig. 2(b). The two curves show the resistance for in-plane fields that are oriented parallel/perpendicular to the current direction. At small fields the AMR dominates the resistance change, as the magnetization can easily be field aligned. At large fields in both geometries a slight, linear decrease in resistance of about $1\times10^{-6}/\mathrm{mT}$ is found. This isotropic behavior is well known as spin-disorder MR.[26] The measurements reveal that MR contributions arising from classical Lorentz MR are not observable. As the fields in the *in situ* MR measurements are small (±23 mT), the spin-disorder MR contribution will be small (≈2 mΩ) and can be neglected compared to the AMR contribution (see below). The dominating AMR effect is given by[26]

$$R(\alpha) = R_{\|} - \Delta R_{\mathrm{AMR}} \cdot \sin^2(\alpha) = R_{\|} - \Delta R_{\mathrm{AMR}} \cdot \frac{M_{\perp}^2}{M_{\mathrm{S}}^2}, \quad (1)$$

where α is the angle between magnetization and current direction, $R_{\|}$ is the resistance for magnetization aligned parallel to the current, and $M_{\perp}$ the magnetization component perpendicular to current direction. ΔR_{AMR} is the difference of resistance for parallel and perpendicular alignment of magnetization with respect to the current direction. For a quantitative discussion of the MR results we have to determine the value of $\Delta R_{\mathrm{AMR}}=\Delta\rho_{\mathrm{AMR}}\cdot l/(w\cdot t)$ for the rectangles. $\Delta\rho_{\mathrm{AMR}}$ describes the maximum resistivity change in the film due to AMR, w and l are the dimensions of the rectangles and t is the thickness of the Py layer. We obtain $\Delta\rho_{\mathrm{AMR}}=(0.39\pm0.02)$ $\mu\Omega$ cm from the *ex situ* four-point MR measurements [see Fig. 2(b)]. Using this value for the nanostructures, we can calculate the maximum resistance change for the two different geometries. When the current runs along the short/long axis, the maximum resistance change is $\Delta R_{\mathrm{AMR,ea}}=(0.10\pm0.01)$ Ω and $\Delta R_{\mathrm{AMR,ha}}=(0.39\pm0.04)$ Ω, respectively.

A. Easy-axis magnetization behavior

The results of the MR measurements for magnetic fields applied parallel to the long axis of the rectangles (the easy axis of magnetization) are shown in Fig. 3. The arrows indicate the field sweep direction. The curves have been obtained in one single field cycle. For all three sizes the same type of resistance versus field curve is found, which demonstrates almost identical magnetization behavior.

Starting at ±23 mT, the resistance increases continuously toward zero field. The change in resistance is 16–20 mΩ. This increase in resistance is due to the AMR effect. Spin-disorder MR effect can be ruled out (see above). The increase in resistance corresponds to $(18\pm3)\%$ of the maximum value $\Delta R_{\mathrm{AMR,ea}}$. At a field of 0.1 mT applied in the opposite direction the resistance jumps by a value of about 19–23 mΩ, corresponding to $(21\pm3)\%$ of $\Delta R_{\mathrm{AMR,ea}}$. The abrupt resistance increase indicates an irreversible magnetization process most likely due to domain nucleation/annihilation. Further increase in the field causes a slight resistance decrease. At a field of 4–9 mT a resistance drop with the same height as the first jump is found. Again, this sudden change in resistance indicates a domain nucleation/annihilation process. The field at which the resistance drops varies slightly from cycle to cycle, while the positive jump

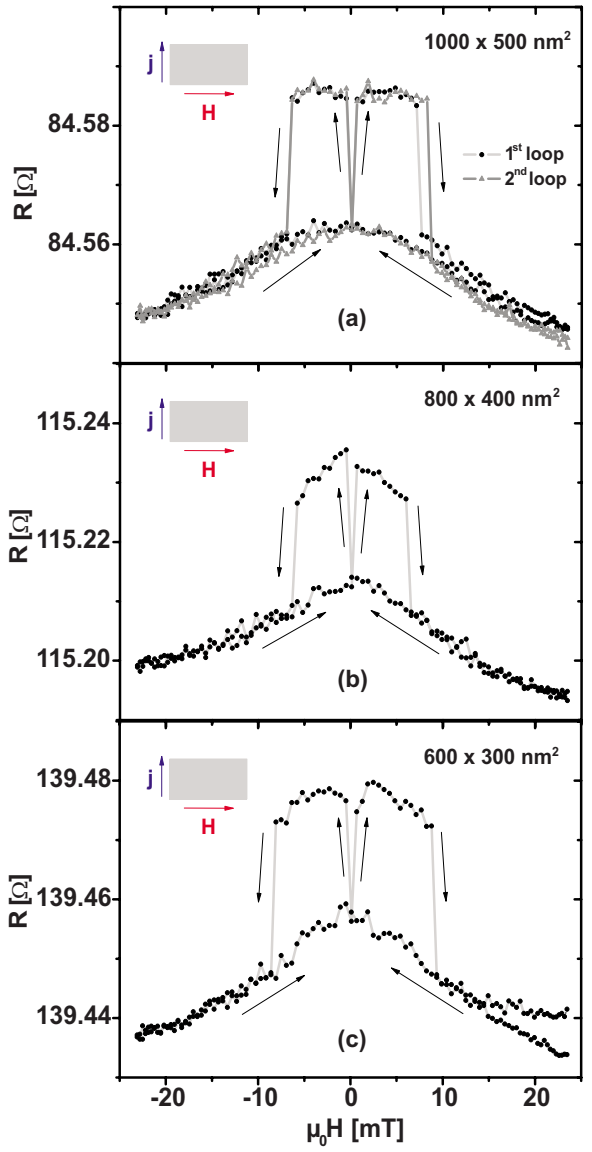

FIG. 3. (Color online) Resistance versus field curves for rectangles with long axis parallel to the field direction. The easy-axis loops for rectangles of size (a) 1000×500, (b) 800×400, and (c) 600×300 nm^2 are plotted. The geometry of the measurement is given as inset.

appears at almost the same field, which is shown in Fig. 3(a), where $R(H)$ curves for two field cycles are plotted.

For the quantitative discussion of the MR measurements information about the magnetic microstructure is necessary. The investigation of the magnetic microstructure in remanence by means of SEMPA reveals that the very same rectangles are either in the C or S state after pretreatment in magnetic fields. In an array of uncoupled rectangles we find that 75 (95/100) out of 100 of the largest (intermediate/smallest) rectangles are in C or S states after the very same pretreatment in magnetic fields. The remaining rectangles exhibit a flux-closure structure, like the Landau or diamond state. From the SEMPA micrographs of the C and S state we can determine the area filling of domains with magnetization parallel to the current direction to be $(27\pm5)\%$. For the Landau and diamond state we obtain $(25\pm6)\%$ and $(50\pm10)\%$, respectively.

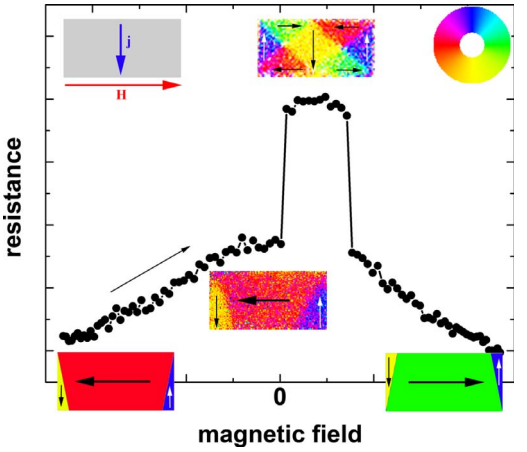

FIG. 4. (Color online) Cartoon of supposed magnetization behavior for fields applied along the easy axis. The domain structures at zero and small positive fields are SEMPA micrographs. The magnetization orientation is color coded according to the given color wheel.

The magnetization behavior of Fig. 3 can be interpreted as follows (see Fig. 4): as the magnetic microstructure in remanence is a C or S state, we can interpret the reversible MR behavior on field decrease either as a reduction in a small tilting of the magnetization of the end domains or as a reversible domain-wall shift that decreases the area of the center domain. The first scenario gives a rotation angle of 54° while in the second situation the area of the end domains has to shrink to $(9\pm5)\%$ at ±23 mT. The relatively high rotation angle of the magnetization in the end domains, which would be accompanied by a considerable increase in magnetostatic energy, indicates that the domain-wall displacement process is the most probable one (see Fig. 4). The latter has been found in micron-sized rectangles before.[27]

The irreversible jump of $(21\pm3)\%$ of $\Delta R_{\mathrm{AMR,ea}}$ at small opposite field indicates that large fractions of the structure exhibit domains with orientation of magnetization along the current direction and perpendicular to the field, respectively. It is reasonable to assume that the system jumps into a flux closure pattern, as the Landau and the diamond state are lower in energy than the C or S states for the dimensions used here.[28,29] As the Landau state would give almost the same resistance as the C/S states, it follows from the resistance jump that the diamond state is created (see Fig. 4). Quantitatively, the height of the jump fits well with the relative difference in area filling of $(23\pm11)\%$ of the parallel to field-orientated domains of the C/S state and the diamond structure normalized to the rectangle area. On further field increase the field degenerated diamond structure is again transformed into the C or S state and a resistance drop appears.

B. Hard-axis magnetization behavior

The results of the MR measurements for magnetic fields applied parallel to the short axis of the rectangle (the hard

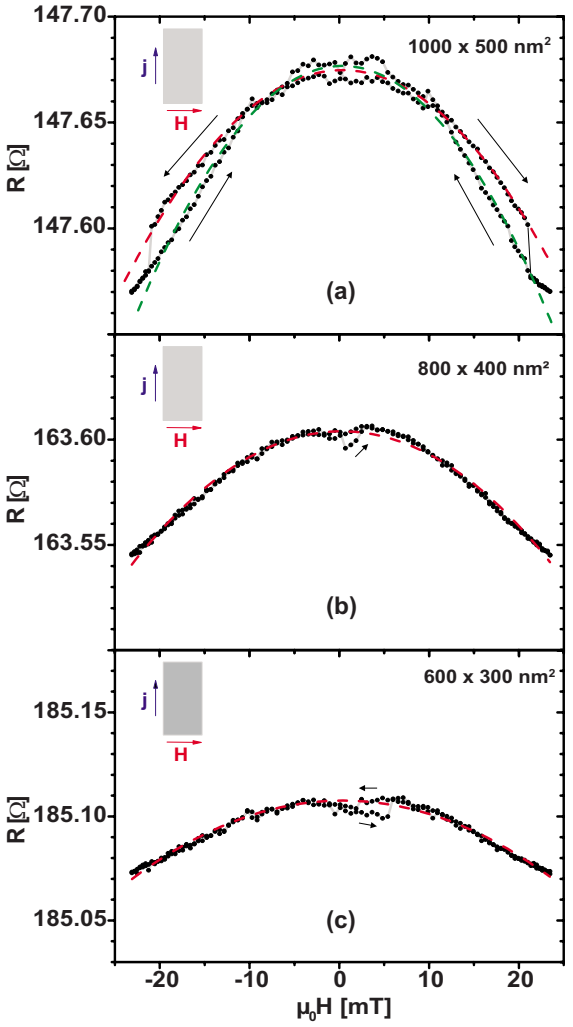

FIG. 5. (Color online) Resistance versus field curves for rectangles with short axis parallel to the field direction. The hard-axis loops for rectangles with dimensions of (a) 1000×500, (b) 800×400, and (c) 600×300 nm^2 are shown. The geometry of the measurement is given as inset. The dashed lines show parabolic fits which indicate (coherent) magnetization rotation during the reversal process.

axis of magnetization) are shown in Fig. 5. For the sake of better comparison the ordinate scales are identical in all plots. The arrows indicate the field sweep direction. The curves have been obtained in one single field cycle.

The same type of parabolic resistance versus field curve is found for all three sizes. Deviations from the parabolic dependence are found around zero field and for the largest rectangle additionally at high fields. The amount of resistance change becomes smaller with shrinking dimensions of the rectangles.

The microstructure in remanence has been obtained via SEMPA. The Landau state is the predominant state for such rectangles, which has been checked for arrays of uncoupled rectangles. After the very same pretreatment in magnetic fields, 60% (90%/99%) exhibit the Landau structure in case of the largest (intermediate/smallest) size. The remaining rectangles show C or S states. From this result we can deduce the following magnetization procedure (see Fig. 6): the

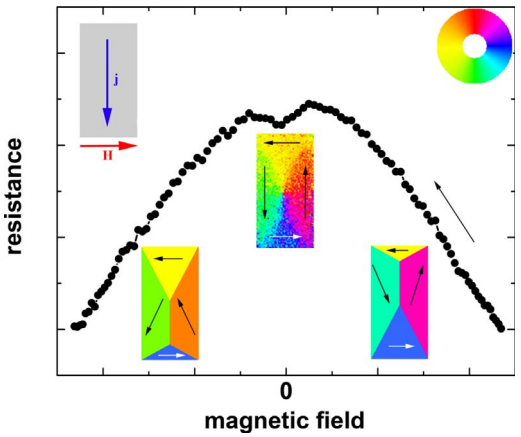

FIG. 6. (Color online) Cartoon of supposed magnetization behavior for fields applied along the hard axis. The domain structure at zero field is a SEMPA micrograph. The magnetization orientation is color coded according to the given color wheel.

Landau state has two large domains that are oriented perpendicular to the field direction, while two small domains at the end have parallel/antiparallel field alignment, respectively. According to Eq. (1), the parabolic field dependence indicates that the magnetization component perpendicular to the current increases linearly with field. When the remanent state is a Landau state, the only mechanism that creates a parabolic MR signal is the rotation of the magnetization of the two large domains. The reason for this assumption is twofold. At first, according to performed simulations[30] the area of the two small oppositely magnetized domains will change by almost the same amount while the one shrinks and the other grows. As both magnetization orientations exhibit the same resistivity, the MR will stay constant within the error margins of the experiment. The second reason is that the Landau state creates stray fields that are caused by a slight tilting of the magnetization in the large domains out of the direction parallel to the long axis.[29,31] External fields along the short axis can easily affect that pre-existing tilting and increase the angle of tilt even at small fields. Hence, a magnetization tilting in the Landau structure occurs.

In the largest structure irreversible changes can be seen at large fields. We appoint that hysteretic behavior to a sudden change in domain structure after the rotation has become so large that a low-angle domain wall can easily be moved and a C/S state is created.

In case the rotation of magnetization is dominant we can calculate from the MR curve the magnetic anisotropy that counterbalances the Zeeman torque. The linear dependence of the magnetization on field is typical for a uniaxial anisotropy. So the equilibrium magnetization orientation in field for a uniaxial system can be put into Eq. (1)

$$R(\mu_0 H) = R_{\parallel} - \Delta R_{\mathrm{AMR,ha}}^{\mathrm{Landau}} \cdot \left(\frac{\mu_0 H M_S}{2K}\right)^2, \qquad (2)$$

where $\mu_0 H$ is the external field, K the first-order uniaxial anisotropy constant, and M_S is the saturation magnetization. $\Delta R_{\mathrm{AMR,ha}}^{\mathrm{Landau}}$ can be determined from the area filling of domains with magnetization perpendicular to the current direction. As

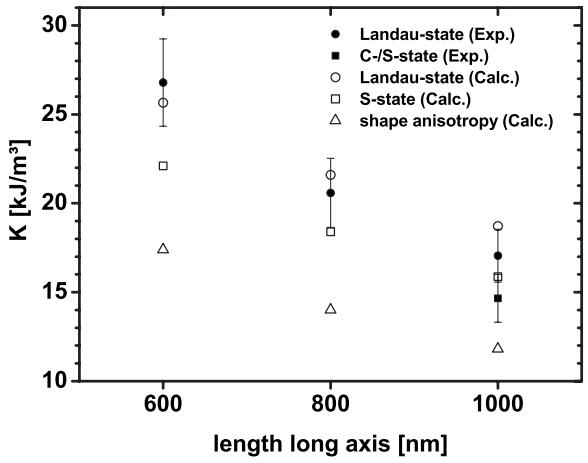

FIG. 7. Anisotropies for different sizes of Py rectangles. The open symbols represent calculated shape anisotropy and calculated energy density differences between the hard-axis saturated state and certain domain structures given as labels in the plot. The filled symbols have been obtained by fitting a uniaxial behavior to the hard-axis curves from Fig. 5.

the large domains of the Landau state occupy roughly 75% of the rectangle we can expect a maximum resistance change of $\Delta R_{\mathrm{AMR,ha}}^{\mathrm{Landau}}=0.75\times\Delta R_{\mathrm{AMR,ha}}=(0.29\pm0.04)\ \Omega$.

The largest structure exhibits a reversible resistance change in about 25% of $\Delta R_{\mathrm{AMR,ha}}^{\mathrm{Landau}}$ when sweeping the field from 0 to 21 mT, i.e., up to the field at which the irreversible jump occurs. This value corresponds to a magnetization rotation of 30°. In case of the smaller structures, the rotation angle at maximum field is 26° (19°) for the intermediate (smallest) rectangle. The smaller rotation indicates a stronger magnetic anisotropy that competes with the Zeeman energy. Finally, we can calculate the first-order anisotropy constant for the different rectangles using a saturation magnetization of $M_S=(820\pm40)$ kA/m, which is determined by means of SQUID measurement. The results are $K=(17\pm2)$ kJ/m^3, [(21 ± 2) kJ/m^3/(27 ± 3) kJ/m^3] in case of the largest [intermediate/smallest] size.

The results for the anisotropy constants should be comparable to the shape anisotropy because the magnetocrystalline anisotropy of the film is very small (300 J/m^3) and the only effective anisotropy is due to the shape. In its strict definition the latter is the difference between the energy of the saturated states along the hard (short) and easy (long) axis. The shape anisotropy has been calculated utilizing an open access micromagnetic simulation code (OOMMF).[30] Experimental results (●) and calculated shape anisotropy values (△) are plotted versus long axis size in Fig. 7. It is obvious that the experimental values do not fit the simulated values. The experimental results are systematically larger, meaning that either there do exist some further contributions to the anisotropy or the nanostructure properties diverge considerably from the assumptions. The properties such as saturation magnetization and size have been cross-checked. As they were identical to the values used for the analysis, an additional contribution to the anisotropy has to be considered. To explore the reason for the systematic deviation, we have calculated the energy density of the micromagnetic states that have been found in the SEMPA investigation. The calculated energy density differences between the hard-axis saturated state and the domain structures, i.e., the S state (□) and the Landau configuration (○), are included in Fig. 7. It is evident that these calculated energy density differences fit the experimental results quite good. For the small and intermediate rectangles the experimental values are very close to the calculated values of the most probable domain configuration, i.e., the Landau state. In particular, it turns out that the anisotropy can be used to distinguish between different domain configurations. One direct proof becomes evident from the magnetization behavior of the largest rectangle, where at higher fields the irreversible change from the Landau configuration to the C/S state is found [see Fig. 5(a)]. In the up and down scans the two different curvatures of the parabola demonstrate that the magnetization rotation in the two states is counterbalanced by different torques, yielding different anisotropies (● and ■ in Fig. 7). For the calculation of the anisotropy utilizing Eq. (2), $\Delta R_{\mathrm{AMR,ha}}^{\mathrm{C/S\ state}}=0.73\times\Delta R_{\mathrm{AMR,ha}}=(0.29\pm0.04)\ \Omega$ is used for the down scan, yielding $K=(15\pm2)$ kJ/m^3. This anisotropy (i.e., the energy density difference to the hard-axis saturated state) of the C/S state is smaller than that of the Landau state, which means that the C/S state is higher in energy as predicted from simulation.[29] Quantitatively, the energy density difference between the C/S state and the Landau state can be obtained from the experiments, yielding (2.4 ± 0.7) kJ/m^3, which fits well the value of 2.8 kJ/m^3 from calculations.

The experimental results reveal the amazing fact that we can measure the magnetic energy of the rectangles. The magnetization rotation is not only affected by the shape anisotropy, which is determined by the surface charges at the rim, but also by the domain state in the same functional dependence. In extended systems domain-wall movement allows to bypass energy maxima, i.e., to take a straight path between two local minima on the energy landscape, as well as transformations via metastable transient states are possible.[32] The complexity of the numerous possible paths makes an exact description of the reversal and the extraction of real numbers nearly impossible. In small structures, however, there does not exist any alternative domain structure that can be reached with small to medium fields. The energy landscape is thus apparently fixed to one minimum for a certain span of external field strengths. The potential gradient, respectively, the torque, is caused by the total energy difference between initial and final state. Surprising is still the fact that our results reveal similar field dependence as a uniaxial anisotropy in lowest-order approximation.

In the discussion we have assumed a homogenous current density within the rectangles. We are aware that the current density would be not exactly homogenous. Different magnetization orientations of the domains cause locally varying current densities, which have to be taken into account. Nevertheless, it has been shown that a uniform electrical current density is a good approximation in microstructures,[33] as the AMR ratio is only a few percent. Using this assumption the resistance contribution of the individual domains depends only on the area filling and magnetization orientation. The influence of the domain walls on resistance has been neglected as the area filling of the walls is vanishingly small.

IV. CONCLUSION

We have investigated the magnetization behavior of single submicron Py rectangles (20 nm thick) via AMR using single field cycles. The magnetization reversal for the two generic cases with the magnetic field applied perpendicular and parallel to the long axis of the rectangles has been explained. Particularly, we can quantify reversible and irreversible magnetization processes. In case of the magnetic field applied parallel to the long axis, the dominating feature is the switching between the quasisingle-domain C/S states and the diamond state. In case of the magnetic field applied perpendicular to the long axis, the parabolic MR behavior can be attributed to a coherent rotation of the magnetization within the large domains of the Landau and C/S state, respectively. The coherent rotation curves are used to determine the first-order anisotropy constant for the individual rectangles. Surprisingly, the anisotropies deviate from pure shape anisotropy. In comparison to calculated energy densities of the involved micromagnetic states, i.e., the Landau and the C/S states, it turns out that in fact the energy density of these states is obtained. Particularly, the difference of the energy density between both states is measured. The results demonstrate that the magnetization rotation is not only affected by the shape but also by the domain configuration, revealing similar field dependence as a uniaxial anisotropy in lowest-order approximation.

ACKNOWLEDGMENTS

We thank S. Pütter and O. Albrecht for SQUID measurements and M. Scholz and G. Hoffmann for AFM investigation. Financial support by DFG via SFB 668 is gratefully acknowledged.

*akobs@physnet.uni-hamburg.de

[1] R. Wiesendanger, Rev. Mod. Phys. (to be published).
[2] W. Wulfhekel and J. Kirschner, Annu. Rev. Mater. Res. **37**, 69 (2007).
[3] G. Rodary, S. Wedekind, D. Sander, and J. Kirschner, Jpn. J. Appl. Phys. **47**, 9013 (2008).
[4] *Magnetic Microscopy of Nanostructures*, edited by H. Hopster and H. P. Oepen (Springer-Verlag, Berlin, 2004).
[5] B. D. Terris and T. Thomson, J. Phys. D **38**, R199 (2005).
[6] W. Wernsdorfer, K. Hasselbach, A. Benoit, B. Barbara, B. Doudin, J. Meier, J. P. Ansermet, and D. Mailly, Phys. Rev. B **55**, 11552 (1997).
[7] S. S. P. Parkin, M. Hayashi, and L. Thomas, Science **320**, 190 (2008).
[8] D. Atkinson, C. C. Faulkner, D. A. Allwood, and R. P. Cowburn, *Spin Dynamics In Confined Magnetic Structures III* (Springer-Verlag, Berlin, 2006), Vol. 101, p. 207.
[9] M. Brands, R. Wieser, C. Hassel, D. Hinzke, and G. Dumpich, Phys. Rev. B **74**, 174411 (2006).
[10] J. E. Wegrowe, D. Kelly, A. Franck, S. E. Gilbert, and J. P. Ansermet, Phys. Rev. Lett. **82**, 3681 (1999).
[11] L. Vila, L. Piraux, J. M. George, and G. Faini, Appl. Phys. Lett. **80**, 3805 (2002).
[12] U. Ebels, A. Radulescu, Y. Henry, L. Piraux, and K. Ounadjela, Phys. Rev. Lett. **84**, 983 (2000).
[13] A. Aharoni, *Introduction to the Theory of Ferromagnetism* (Oxford University Press, New York, 1996).
[14] T. Wang, Y. Wang, Y. Fu, T. Hasegawa, F. S. Li, H. Saito, and S. Ishio, Nanotechnology **20**, 105707 (2009).
[15] R. A. Silva, T. S. Machado, G. Cernicchiaro, A. P. Guimarães, and L. C. Sampaio, Phys. Rev. B **79**, 134434 (2009).
[16] R. Hertel, J. Magn. Magn. Mater. **249**, 251 (2002).
[17] H. Forster, T. Schrefl, W. Scholz, D. Suess, V. Tsiantos, and J. Fidler, J. Magn. Magn. Mater. **249**, 181 (2002).
[18] R. P. Cowburn, A. O. Adeyeye, and M. E. Welland, Phys. Rev. Lett. **81**, 5414 (1998).
[19] J. Y. Cheng, W. Jung, and C. A. Ross, Phys. Rev. B **70**, 064417 (2004).
[20] D. Stickler, R. Frömter, W. Li, A. Kobs, and H. P. Oepen, Rev. Sci. Instrum. **79**, 103901 (2008).
[21] A. Perin, R. Gupta, G. Principi, C. Tosello, L. M. Gratton, E. Kuzmann, and Z. Klencsar, Surf. Coat. Technol. **103-104**, 93 (1998).
[22] J. Fassbender, J. von Borany, A. Mucklich, K. Potzger, W. Moller, J. McCord, L. Schultz, and R. Mattheis, Phys. Rev. B **73**, 184410 (2006).
[23] T. Miyazaki and T. Ajima, J. Magn. Magn. Mater. **81**, 91 (1989).
[24] A. Yamaguchi, T. Ono, S. Nasu, K. Miyake, K. Mibu, and T. Shinjo, Phys. Rev. Lett. **92**, 077205 (2004).
[25] *Magnetic Microscopy of Nanostructures*, edited by H. Hopster and H. P. Oepen (Springer-Verlag, Berlin, 2004), Chap. 7.
[26] T. R. McGuire and R. I. Potter, IEEE Trans. Magn. **11**, 1018 (1975).
[27] J. M. Garcia, A. Thiaville, J. Miltat, K. J. Kirk, and J. N. Chapman, J. Magn. Magn. Mater. **242-245**, 1267 (2002).
[28] R. Hertel, Z. Metallkd. **93**, 957 (2002).
[29] W. Rave and A. Hubert, IEEE Trans. Magn. **36**, 3886 (2000).
[30] M. Donahue and D. Porter, OOMMF User's Guide, Version 1.0, National Institute of Standards and Technology, Interagency Report No. NISTIR 6376, 1999 (unpublished).
[31] S. Hankemeier, R. Frömter, N. Mikuszeit, D. Stickler, H. Stillrich, S. Pütter, E. Y. Vedmedenko, and H. P. Oepen, Phys. Rev. Lett. **103**, 147204 (2009).
[32] G. Bertotti, *Hysteresis in Magnetism* (Academic, New York, 1998).
[33] M. Bolte, M. Steiner, C. Pels, M. Barthelmess, J. Kruse, U. Merkt, G. Meier, M. Holz, and D. Pfannkuche, Phys. Rev. B **72**, 224436 (2005).